American Mineralogist, Volume 91, pages 1188–1196, 2006

Vibrational spectroscopy of brucite: A molecular simulation investigation

PAUL S. BRATERMAN[1,*] AND RANDALL T. CYGAN[2]

[1]Department of Chemistry, University of North Texas, P.O. Box 305070, Denton, Texas 76203, U.S.A.
[2]Geochemistry Department, Sandia National Laboratories, Albuquerque, New Mexico 87185-0754, U.S.A.

ABSTRACT

We have modeled the vibrational spectrum of brucite, the common phase of magnesium hydroxide, at 1 bar (10^5 Pa) by two separate techniques: molecular dynamics simulation and vibrational mode analysis. Molecular dynamics simulation of a model supercell provides information (from the power spectrum of the atomic velocity autocorrelation function) about the frequencies and directions of atomic thermal motions, using a defined energy force field. Vibrational mode analysis gives complementary information about the frequencies, nature, and infrared and Raman activity of the computed modes of the same system. Using both methods we find (in addition to the spectroscopically active modes) inactive modes up to around 1000 cm^{-1}, corresponding to MOH bending (OH rotational) motions. We invoke these modes to explain the published inelastic neutron scattering data, and suggest that their relatively high frequency is an inevitable consequence of repulsive interactions between neighboring H atoms.

Keywords: Brucite, magnesium hydroxide, infrared, molecular dynamics, neutron scattering, vibrational spectra

INTRODUCTION

In this paper, we use two computational methods (molecular dynamics simulation and vibrational mode analysis) to examine the vibrational motions of brucite, $Mg(OH)_2$, at 1 bar, compare the results with those of traditional factor group analysis, and apply our findings to the interpretation of the experimental data for brucite, and, in particular, to the differences between the results of spectroscopy and those of inelastic neutron scattering. The results supplement those of the usual factor group analysis. Such an analysis gives the modes of the unit cell, which include all the infrared- and Raman-active modes of the solid, but these correspond only to the $k = 0$ vibrations, and turn out to be rather atypical.

Molecular simulations have been extensively applied to mineral systems in general (Cygan 2001), and to metal hydroxides and layered double hydroxides (LDH), in particular (Newman et al. 2001; Wang et al. 2003). Recently, we became interested in applying the technique to understand the effect of M^{2+}:M^{3+} ratio in LDH, and conducted investigations of brucite as a way of validating the methodology. At this stage, we were surprised to discover that there are still outstanding issues regarding the brucite vibrational spectrum, and we are therefore reporting the results of our simulations, in the hope of shedding light on these, and, more generally, on the relationship between the results of different methods of investigation of mineral vibrations.

The vibrational behavior of brucite was discussed in detail, from both a group theoretical and an experimental perspective, in Mitra's (1962) classic review, and has been the subject of numerous investigations since (e.g., Buchanan et al. 1963; Safford et al. 1963; Dawson et al. 1973; Kruger et al. 1989; Lutz et al. 1994; Weckler and Lutz 1996; Chakoumakos et al. 1997; Frost and Kloprogge 1999; de Oliveira 2001; Pracht et al. 2003; Ugliengo et al. 2004). Ryskin (1974) reviews the earlier work, and compares brucite with other hydroxides and oxyhydroxides. The relevant issues include the role of combination bands in adding complexity to the spectrum, the need to allow for the effects of contamination, especially in mineral specimens, and the nature of the hydrogen motions responsible for neutron scattering, which does not obey a symmetry-based selection rule. Further interesting questions arise regarding the effects of pressure, but we do not consider those here. Nor are we able to consider the combination bands found by many authors in the OH stretching region, since our methodology gives fundamentals only.

In molecular dynamics simulations of solids, periodic boundary conditions are imposed on a block of atoms, which for relatively simple materials, such as brucite, are chosen to be a supercell several times larger than the crystallographic unit cell. Within this simulation cell, the individual atoms are treated as classical particles, moving under the influence of a combination of covalent, electrostatic, and van der Waals forces. In the particular energy force field that we use, there is no explicit inclusion of hydrogen bonding (the possible role of which in brucite remains a matter for discussion; e.g., Kruger et al. 1989), since it is fully described by electrostatic interactions and dispersion forces. This is in accord with current views (Desiraju 2002), which assign an additional role to covalent interactions only in the case of the strongest hydrogen bonds. A potentially more serious drawback is the absence of angular constraints on the metal hydroxide bond, other than those imposed by Coulomb forces, despite the partially covalent nature of the Mg-O bonds in brucite.

As pointed out by Cygan (2001) and Kubicki (2001), and the earlier work cited there, the Fourier transform of the atomic velocity autocorrelation function provides information about the

* E-mail: psb@unt.edu

0003-004X/06/0007–1188$05.00/DOI: 10.2138/am.2006.2094

vibrations of the system, which are in effect analyzed as the sum of a spectrum of harmonic vibrations. Separate information can be obtained about all six independent geometric components. For a layered material such as brucite, or any system containing C_3 or higher symmetry, the *xx* and *yy* components of the spectrum should ideally be equal, but in general distinct from the *zz* component, and cross terms should algebraically sum to zero. This is not achieved in actual dynamics simulations, because of thermal noise, but we do not consider these cross terms further.

METHODS

Group theoretical analysis

We follow the approach described by Mitra (1962), while emphasizing bonding interpretations and individual atomic motions. The possible vibrational modes of a regular crystalline solid may be found using the technique of factor group analysis, in which a crystalline space group is broken down into a translational group, and a "factor group" that describes the symmetry of the unit cell, translationally equivalent atomic sites being regarded as identical. More exactly, the space group is treated as the Cartesian product of the translational group and the factor group. For brucite, the factor group is D_{3d}; this designation ignores the slight displacements of the H atoms from their special positions suggested by some authors (see Chakoumakos et al. 1997; Desgranges et al. 1996). The analysis proceeds in much the same way as the familiar point group analysis of the possible motions of isolated molecules (see e.g., Cotton 1990), but with some important differences:

(1) An object contributes to the character of the matrix representing an operation if that operation turns the atom concerned back into itself, *or into a translationally equivalent object*. Thus the O atoms in brucite are treated as invariant under C_3, which converts each one into its translational equivalent, but not of course under S_6, which interconverts the translationally non-equivalent upward- and downward-pointing O atoms. (2) In solids, the modes of the different unit cells can be combined together in a large number of ways, corresponding to phase shift vectors, so that an individual mode of the unit cell gives rise to a band of related modes over the crystal as a whole. In spectroscopic analysis, this fact is generally ignored, since it is only the $k = 0$ mode that is active. This is true in both infrared and Raman spectra. If $k \neq 0$, then potential activity (oscillating dipole, or change in polarizability) in one part of the crystal will be canceled out in another part. However, as we shall see, the entire range of modes needs to be considered in a more comprehensive analysis, especially in a lattice that is held together by ionic or covalent forces.

(3) In isolated molecules, three modes are simply discarded as representing free translations, or acoustic modes, and three (two for a linear molecule) as free rotations. In tightly bound solids, these motions (except for the $k = 0$ component which represents motion of the crystal as a whole) represent genuine, although spectroscopically inactive, distortional modes.[1]

The composition of the (possibly idealized) unit cell is $Mg(OH)_2$, giving a total of fifteen independent atomic motions; three Mg translations, two hydroxide stretching motions, four hydroxide group rotations or librations, and six hydroxide group translations. Of these, three modes are assigned as overall translations, and are generally not considered further (see the comment and footnote above). It is convenient for our purposes to relate these various modes to atomic motions in the *z* or in the *x*,*y* directions, as in Table 1.

Four infrared active modes are predicted. The OH stretch, and the out-of-plane OH translation (an Mg-O stretch but with some implied bend character) transform as A_{2u} and will be *z*-polarized, while the in-plane OH translation (mainly an Mg-O bend, but with some stretching) and the OH rotation (or Mg-OH bend) both transform as E_u and will be *x*,*y*-polarized. Modes of the same symmetry can in principle mix. A Raman active partner is predicted for each infrared mode because motions of O, H can be taken in phase or out of phase within the unit cell.

It is essential to note that for the brucite crystal as a whole this analysis predicts, not the number of possible vibrational modes, but the number of translationally related families, each of which will give rise to as many components as there are units in the crystal; however, only the $k = 0$ member can be spectroscopically active.

Structural model, computational details, and force field

Atomic interactions are described in our molecular dynamics simulations by the CLAYFF force field (Cygan et al. 2004). It should be noted that this force field was developed without regard to the accurate modeling of vibrational spectra, and, in particular, that it is likely to underestimate directional effects (see Introduction). The force field was used in conjunction with the OFF energy program and the Cerius[2] molecular modeling software package (Accelrys Inc., San Diego, California). An idealized unit cell of brucite constructed according to the structure determination of Zigan and Rothbauer (1967) was used as the initial building block for a supercell containing 144 units ($8 \times 6 \times 3$ along *a*, *b*, *c* cell vectors respectively). Figure 1 provides a ball and stick model of the unit cell of brucite along with the supercell representation to better visualize the layered structure.

For the velocity autocorrelation function determination, the supercell was thermally equilibrated as an isothermal-isobaric (*NPT*) statistical ensemble at 100 and 300 K for a minimum of 20 ps. Long-range electrostatics interactions for the periodic cells were evaluated using the standard Ewald summation method (Tosi 1964), and a spline cutoff was used with values of 8.0 and 8.5 Å to obtain the short-range non-Columbic energies. A Verlet (1967) algorithm was used to integrate the equations of motion for each of the 1 fs time steps. The molecular dynamics simulations utilize the Hoover (1985) thermal transfer algorithm to maintain a constant temperature for the system, and the Parrinello-Rahman method (Parrinello and Rahman 1981) to control the hydrostatic pressure at a nominal 10^5 Pa (effectively zero pressure, since this value is considerably smaller than the thermal fluctuations). The atomic motions were then followed for 40 ps of additional dynamics while recording trajectories that include structures and atomic velocities every 2 fs.

For the investigation of vibrational modes, the potential energy of the unit cell was minimized according to the force field, with no symmetry constraints (*P*1 symmetry), a range of supercells ($2 \times 2 \times 2$; $8 \times 6 \times 3$; $5 \times 5 \times 5$) were constructed from this, and the vibrational modes of both the energy-minimized unit cell, and the unit cells constructed from it, were then calculated using periodic boundary conditions. While symmetry constraints were relaxed during these calculations, only negligible deviations among the supercell models were observed, and the supercell energies were equal to, or negligibly less than, the appropriate multiple of the optimized unit-cell energy. We followed this procedure, rather than starting from a thermally equilibrated model, to avoid freezing-in distortions. Vibrational frequencies are obtained from the minimized brucite model using a quasi-harmonic approximation and the Hessian matrix involving the second derivative of the potential energy (Born and Huang 1954). Infrared intensities are derived from the summation of the product of the partial charge and the displacement vector for each atom.

In addition to calculated frequencies, this procedure yields a graphical mode analysis within the Cerius[2] interface, which was used to determine the nature of the atomic motions in the calculated modes. All modes of the unit cell and $2 \times 2 \times 2$ supercell were inspected visually, as were a sampling of modes from the larger supercells. Calculations were performed on either a single processor Fuel or dual-processor Octane SGI Unix workstation. The molecular dynamics runs for the largest supercell took approximately 27 h, while the vibrational analyses typically took less than 30 min to complete.

RESULTS AND DISCUSSION

Results of vibrational mode analysis

Minimizing the potential energy of the unit cell of brucite gave no detectable distortion from ideal symmetry, and further changes on minimizing the energies of the supercells were negligible. The structure of the energy-minimized unit cell is in excellent agreement with the published structure of Zigan and Rothbauer (1967). Although minimized without constraint—constant pressure and *P*1 symmetry—the optimized cell exhibits the observed trigonal $P\bar{3}m1$ space group and has cell parameters in agreement (approximately 2% difference) with the experimental determination (simulation: $a = b = 3.220$ Å, $c = 4.672$ Å; $\alpha = \beta = 90°$, and $\gamma = 120°$; experimental: $a = b = 3.142$ Å, $c = 4.766$ Å; $\alpha = \beta = 90°$, and $\gamma = 120°$). There was no evidence in any of the energy-minimized cells for the suggested (Desgranges et al.

[1] To see this, redefine the unit cell so as to double its size. The in-phase combination over the two parent cells of a rotational or translational mode will retain the same identity in the enlarged cell, while the out of phase combination will correspond to a distortion in which the two original components are moving in different directions.

TABLE 1. Vibrational modes of $Mg(OH)_2$, classified under the D_{3d} factor group

Representation	Group motion	Bonding interpretation	Activity	Principal atomic motion(s)
A_{1g}	OH stretch	OH stretch	R	H (minor O)
	OH translation	MgO stretch (bend)	R	H, O
A_{2u}	Mg translation	Cell translation	T	All
	OH translation	MgO stretch (bend)	IR (*z*)	H, O, Mg
	OH stretch	OH stretch	IR (*z*)	H (minor O)
E_g	OH rotation	MgOH bend	R	H (minor O)
	OH translation	MgO bend (stretch)	R	H, O
E_u	Mg translation	Cell translation	T	All
	OH rotation	MgOH bend	IR (*x*,*y*)	H (minor O)
	OH translation	MgO bend (stretch)	IR (*x*,*y*)	H, O, Mg

Notes: R = Raman-active; IR = (*z*), infrared-active (*z*-polarized) etc; T = cell translation (acoustic mode; inactive).

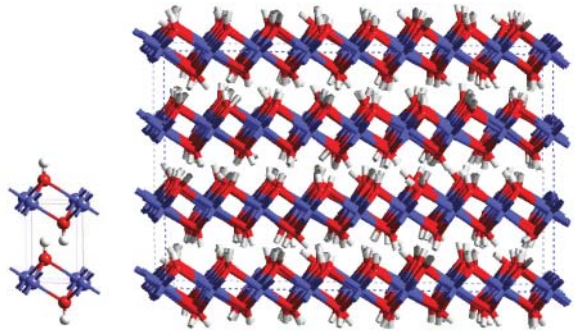

FIGURE 1. Crystal structure of brucite presented as energy minimized unit cell and snapshot for $8 \times 6 \times 3$ structure from equilibrated molecular dynamics *NPT* simulation.

1996) deviation of the H atom positions from sites of threefold symmetry.

The results of the unit-cell vibrational analysis are shown in **bold** in Table 2. The modes obtained correspond to the group theoretical predictions (it would be strange if they did not). Noteworthy features include the very low frequency for the E_u OH rotation (MOH bending) mode, which is presumably an artifact of the force field, the large separation between E_u and E_g modes of this type (reflecting the strength of interlayer H-H charge repulsion), the small contribution to the overall intensity of the A_{2u} *z*-axis OH translation (MO stretch/bend), and the absence of any strong noticeable mixing between OH translational and rotational modes of the same symmetry type. However, the amplitudes of motion suggest some mixing within our model of E_g OH librations and translations.

The $2 \times 2 \times 2$ supercell gives rise to a total of 120 modes (also incorporated into Table 2), including the three simple translations. In the simplest cases, these are combinations of modes of the unit cell, taken in or out of phase between neighbors in each of the three directions possible, so that each mode of the unit cell would give rise to eight modes in the supercell. In reality, however, more complicated motions also result since different phase combinations of different simple modes can have the same overall symmetry, and this can be important in determining the density of vibrational states. The only spectroscopically active modes are those directly corresponding to $k = 0$ combinations of the unit cell, and occurring at the same frequency. However, the other modes illustrate the full range of possible effects of neighboring units on each other, and the spread produced by these effects will be essential to the interpretation of the vibrational modes and molecular dynamics of the larger model systems (and by implication of actual crystals), and to the interpretation of the neutron scattering data.

For obvious reasons, we do not attempt to present all the possible modes of the larger supercells, but content ourselves with showing the density of states, as defined by the number of states between $x + 5$ and $x - 5$ cm^{-1}, collected at 5 cm^{-1} intervals (results for the $8 \times 6 \times 3$ supercell are shown in Fig. 2). Although the modes of the original unit cell are, as they must be, preserved intact, they do not in general correspond to conspicuous features of this plot. The modes around 3600 cm^{-1} correspond, as expected, to almost pure OH vibrations, but no such simple description is possible for the extremely broad distribution found at lower frequencies. Here, both the highest and lowest ends correspond to OH (*x*,*y*) rotations (i.e., MOH bending motions), but throughout the body of the distribution these are interspersed with motions of other types, and motions of mixed type are common. The specific modes found are, of course, dependent on the chosen dimensions of the supercell; for example, in this supercell, the adjacent layers are constrained to be $2\pi/3$ out of phase with each other. The constraints on a $5 \times 5 \times 5$ supercell are accordingly different, corresponding to different periodicity constraints (Fig. 3). Thus, in a real crystal, which is much larger than any of our model supercells, the distribution will be that much smoother, and care must be taken to avoid over-interpreting the results for any particular chosen supercell.

Several important features are evident when comparing the single unit-cell and supercell computations:

(1) The preservation unchanged, as expected, of all the single cell modes as in-phase repeats (corresponding to $k = 0$ modes of a real crystal) in each supercell calculation. Note, however, that the positions of these modes do *not* correspond to regions of high density of vibrational states in the supercell or, by implication, in the actual crystal.

(2) The increase in the total number of modes, as expected.

(3) Specific to the $2 \times 2 \times 2$ supercell, the occurrence of many modes in families of three, although the factor group symmetry (D_{3d}) imposes at most twofold degeneracy. We regard the threefold degeneracies as pseudo-accidental, arising from the high symmetry of the translational repeat unit.

(4) The existence of mixed modes.

(5) The spreading out of frequencies and splitting into bands. Here, the exact details differ between different supercells, but they all have several significant features in common: the formation of a structured band between 50 and 450 cm^{-1}, with maximum around 150, 250, and 350 cm^{-1}, a minimum or gap between

TABLE 2. Summary of calculated modes for $2 \times 2 \times 2$ supercell

Frequency cm^{-1}	Number*	Description†	Main atomic motions, directions
3738.6	**1**	**A_{2u} OH stretch**	**H, z**
3678.3	**1**	**A_{1g} OH stretch**	**H, z**
Other OH stretches at 3806.9(1), 3714.0(3), 3706.9(3), 3693.1(3), 3690.6(3), 3678.2(1) (mainly H-atom *z*-directed motion)			
MOH bends at 930.8(3), 909.9(3), 811.6(3), 808.6(3) (mainly H-atom *x*,*y*-directed motion)			
703.3	**2**	**E_g MOH bend**	**H, x y**
702.2	2	MOH bend	H, x y
540.8	3	MOH bend + some T_z(OH)	H, x y + some H, O, z
529.7	3	MOH bend	H, x y
520.1	1	MO stretch-bend	H z, O z, Mg z
435.5	**1**	**A_{1g} MO stretch-bend**	**H z, O z**
373.5	**1**	**A_{2u} MO stretch-bend**	**H z, O z, Mg z**
373.0	3	Mixed OH translations	H x y z, O x y z, Mg x y
361.4	3	MO bend/stretch + MOH bend	H x y, O x y
357.1	3	MO bend/stretch + stretch/bend	H x y, some z, O x y, some z
353.0	3	MO bend/stretch + Mg z-motion	H x y, O x y, Mg z
344.4	1	MO stretch/bend	H z, O z
338.3	3	MO bend/stretch + MOH bend	H x y, O x y, Mg x y
337.9	3	MO bend/stretch + MOH bend	H x y, O x y
329.3(3), 320.7(2)		MO bend/stretch	H x y, O x y, Mg x y
316.8	**2**	**E_u MO bend-stretch**	H x y, O x y, Mg x y
313.0	3	MO stretch/bend + bend/stretch	H x y z, O x y z, Mg x y
304.4	3	MO bend/stretch	H x y, O x y
261.9	3	MO stretch/bend + bend/stretch	H x y z, O x y z, Mg x y
252.5	3	MO stretch/bend + bend/stretch	H x y z, O x y z
246.1	**2**	**E_g MO bend-stretch**	**H x y, O x y**
241.8(3), 228.8(2), 226.3(3)		MO bend/stretch	H x y, O x y
222.7	3	T(OH), R(OH) all mixed	H x y z, O x y z
182.0	1	MO stretch/bend	H z, O z, Mg z
172.6(3), 168.4(3)		MO stretch/bend + bend/stretch	H x y z, O x y z
168.4	3	MO stretch/bend + bend/stretch	H x y z, O x y z
163.2(3), 162.7(3)		MO bend/stretch	H x y, O x y, Mg x y
85.8	2	MOH bend	H x y
84.69	**2**	**E_u MOH bend**	**H x y**
0.4 to 0.2	**3**	**Overall translation**	**Frequency ideally zero**
–295.1(3), –296.6(3)		MOH bend	Frequency is computational artifact

Notes: The $k = 0$ modes, which also occur in the analysis of a single repeat cell, are shown in **bold**.
* For discussion of threefold pseudo-accidental degeneracies, see text.
† MOH bend = OH libration; MO stretch/bend = OH *z*-directed translation; MO bend-stretch = OH *x*,*y*-directed translation.

450 and 525 cm^{-1}, a spreading out of frequencies through the region 700–1000 cm^{-1}, and the appearance of two density maxima in the OH stretching region. Note that the interaction between OH groups in the same layer is suppressed in the treatment of the individual unit cell, where these groups are constrained to move in phase, but not in the supercell calculations. Thus we can attribute the states between 700 and 1000 cm^{-1}, for example, to vibrations in which adjacent OH groups in the same layer are moving out of step and repelling each other.

(6) The nature of the vibrational modes as a function of frequency. There are 6, 124, and 143 modes at negative frequencies for the $2 \times 2 \times 2$, $5 \times 5 \times 5$, and $8 \times 6 \times 3$ supercells, respectively. Such negative frequencies are evidently an artifact of the frequency calculation algorithm. The success of the energy minimization procedure ensures that all force constants are positive and all frequencies real.

The region above 3600 cm^{-1} is immediately assignable to OH stretching motions. In all supercells, there is a markedly bimodal distribution, with the calculated Raman-active mode near the lower end of the frequency range, the infrared-active mode near the top, and a total range of up to 150 cm^{-1}.

The OH (*x*,*y*) rotations, which we would prefer to describe as MOH bending modes, span the entire range from the lowest frequencies up to approaching 1000 cm^{-1}. The separation between the infrared active mode and the Raman active mode is due to repulsive interactions between H atoms at the top of one layer, and those at the bottom of the layer above it (see Fig. 1). The additional observed spread is due to repulsions within each layer. The extreme breadth of this feature is clearly attributable to strong repulsions between similarly charged H atoms moving toward each other. The OH translations (both *z*- and *x*,*y*-oriented; these can be considered as Mg-O bending/stretching modes), with in some cases associated Mg motions, occur at various frequencies between 450 and 300 cm^{-1}, in which region mixing of modes of different types is common. These conclusions are summarized in Table 3a.

Results of molecular dynamics simulation

Attempts to carry out molecular dynamics simulations on a single unit cell led to unrealistic distortions due to the local imbalance of forces on a small-scale molecular system. This is enhanced by the fact that each atom is formally its own neighbor, leading to an unrealistic feedback. Meaningful and reasonably similar results were however obtained from the $2 \times 2 \times 2$ simulation, as well as $5 \times 5 \times 5$ and $8 \times 6 \times 3$, simulated at 300 K, and for $8 \times 6 \times 3$ simulated at 100 K, as *NPT* statistical ensembles. The results are summarized in Table 4 and vibrational data for the $8 \times 6 \times 3$ supercell at 300 K presented in Figure 4. We had expected that a simulation at 100 K would give rise to better resolution than at higher temperature, but this was not the case.

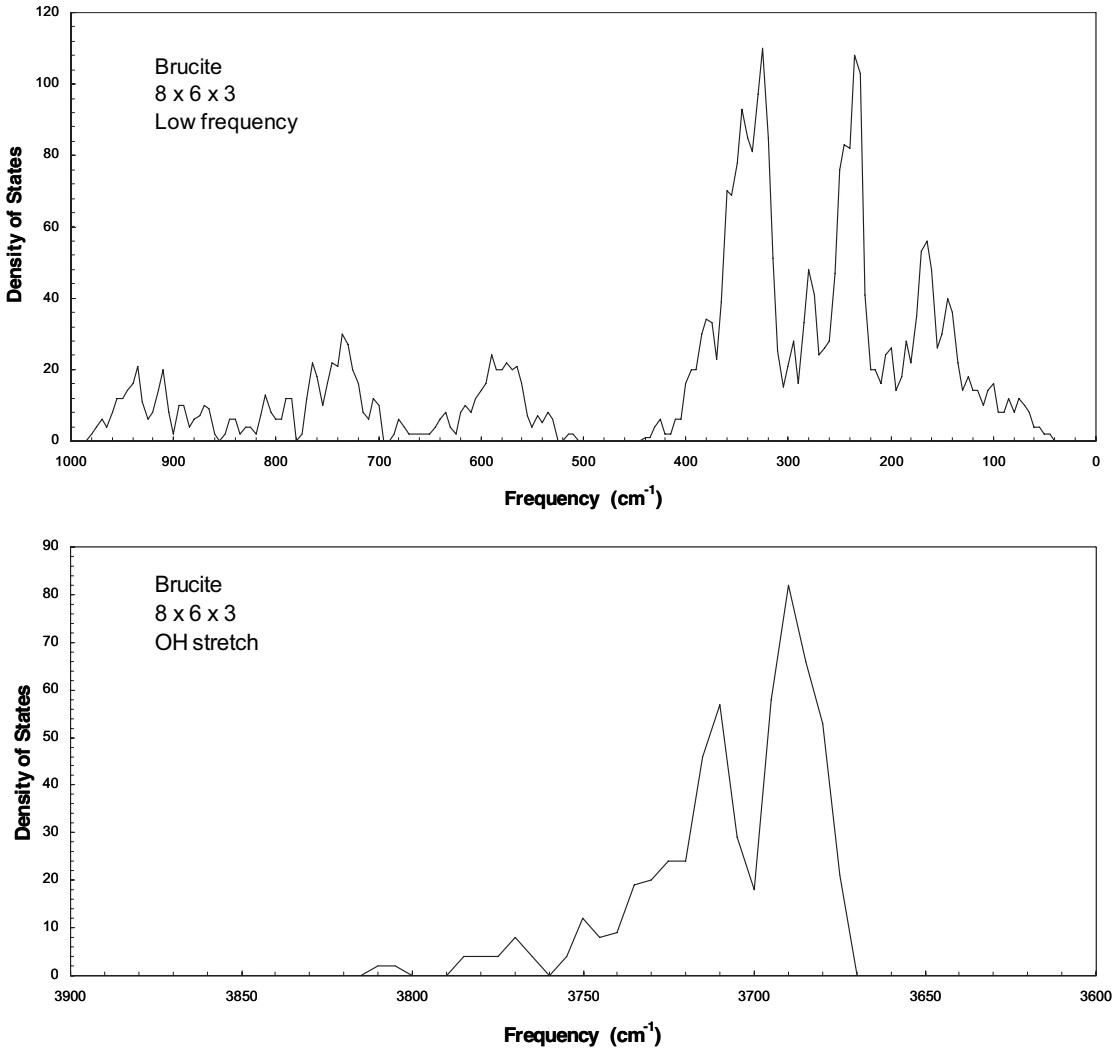

FIGURE 2. Density of computed vibrational states in $8 \times 6 \times 3$ supercell of brucite.

TABLE 3. Assignments of atomic motions within model

Motion	Supercell values	
	(**a**) Vibrational frequencies	(**b**) From power spectra
OH stretch	3680–3800 (max. 3690, 3710)	3750–3830 (max. 3760, 3790)
MOH bend = R(*x*,*y*)OH)	60–975	0–1000
MO bend/stretch = T(*x*,*y*)OH	125–410	120–400 (max. 150, 220, 320)
MO stretch/bend = T(*z*)OH	170–590	120–400 (max. 130, 230, 340)

We derive the assignments of Table 3b as follows:

There are only three kinds of atoms to consider. Motions heavily concentrated on H only are assigned as OH stretching or OH (*x*,*y*) rotation (MOH bending). The OH stretching motions should be *z*-polarized while the MOH bends are *x*,*y*-polarized.

Motions concentrated on O should correspond according to polarization to T(*z*)(OH), or T(*x*,*y*)OH, displacements of the hydroxide group (MO stretching/bending motions). These should involve comparable displacements of H.

Motions concentrated on Mg should correspond to unbalanced combinations of OH translations, that is, combinations in which there is displacement of the center of mass of the OH groups taken as a whole.

In addition, there may be low-frequency motions affecting all atoms equally, related to displacements of the fundamental simulation cell.

More than one kind of motion may contribute in a given frequency range. In such a case, it is not possible for us to distinguish from the power spectra alone between truly mixed modes (modes involving more than one kind of atomic motion), and frequency overlap between groups of unmixed modes, although we know from the results of the previous section that both of these can occur.

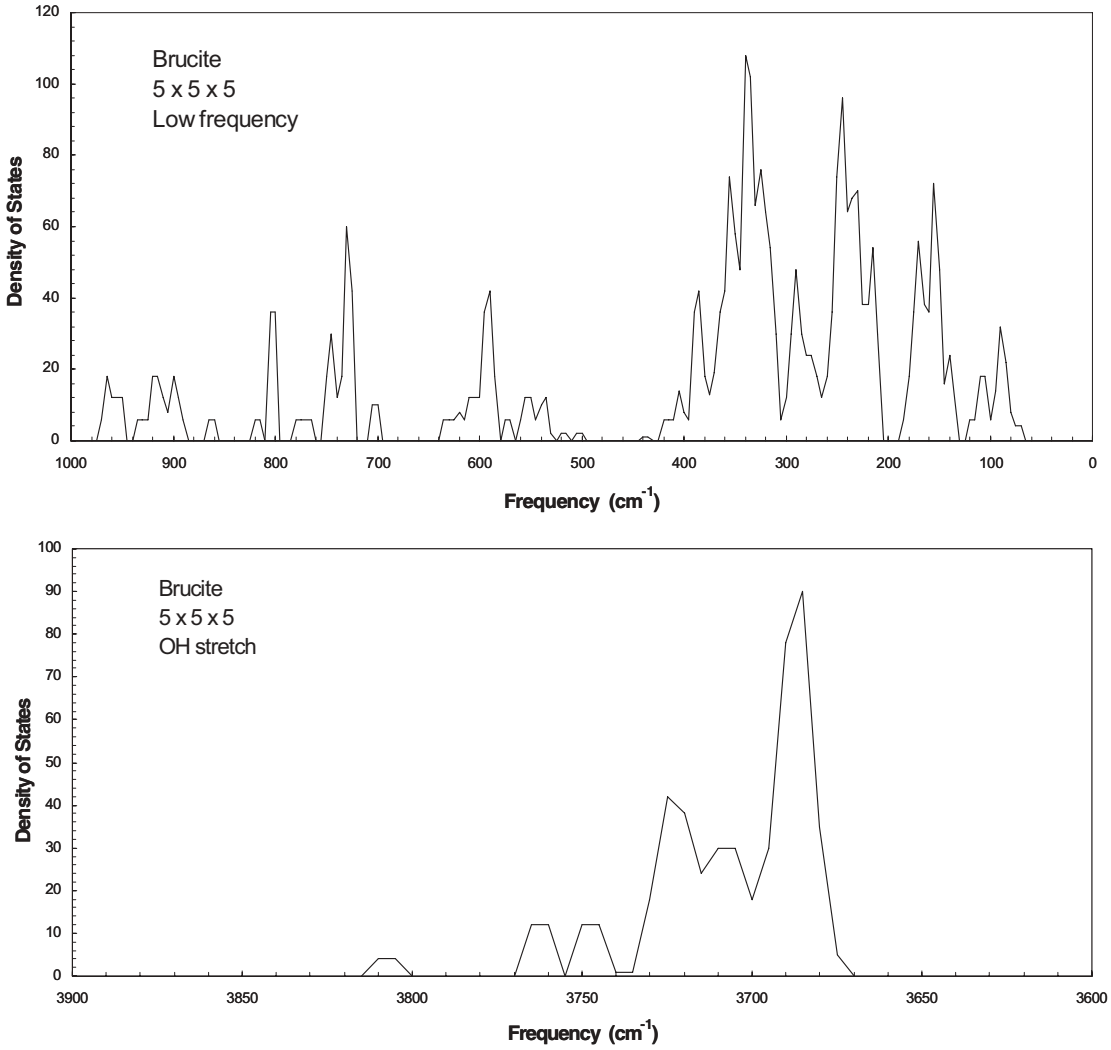

FIGURE 3. Density of computed vibrational states in $5 \times 5 \times 5$ supercell of brucite.

TABLE 4. Simulated atomic motions

Atom type	Cell	*x*,*y* - peaks	*z*-peaks
Mg	2×2×2	145(2.5), 290(5.5)	145(3.7)
	5×5×5	81(0.3), 150(0.9), 210(1.1), 295(1.1,br)	84(0.2), 140(1.4), 305(0.4)
	8×6×3	175(0.6), 300(1)	140(1.4), 305(0.4)
	8×6×3 (100 K)	95(0.02), 185(0.09), 280(0.1), 360(0.08)	158(0.25), 330(0.04)
O	2×2×2	150(2.3), 200(4.8), 325(3.0)	140(0.3), 250(1.0), 325(2.0)
	5×5×5	82(0.2), 150(1.0), 220(2.8), 315(2.4)	84(0.2), 128(0.4), 230(0.8), 335(1.1)
	8×6×3	180sh(0.6), 225(2.6), 315(2)	130(0.3), 225(0.6), 340(1.2)
	8×6×3 (100 K)	170sh(0.1), 240(0.35), 350(0.2)	140(.03), 250(.07), 370(.14)
H	2×2×2	145(40), 300br(20), 650(95), 945(90)	3760(5000), 3780(3500)
	5×5×5	150-320(20), 705(50), 900(60)	3760(2200), 3785(1000)
	8×6×3	140-320(20), 690(50), 900(60), 3760(5)	3763(3500), 3783(2500)
	8×6×3 (100 K)	200-400br(1.0), 635(6), 800(7), 910(9), 1035(4), 3740(3)	420(0.5), 515(0.3), 800(0.3), 935(0.8), 3780

Notes: Frequency in cm^{-1}. Intensity in arbitrary units; (*xx*+*yy*) and *zz*, respectively.

Immediately and unsurprisingly, the peaks around 3760 and 3780 cm^{-1} are assignable as OH stretching motions. Peaks in the range 600–1000 cm^{-1} are assignable as MOH bends, which must also contribute to the region between 100 and 400 cm^{-1}, since the amplitude of H atom *x*,*y*-polarized motion is greater than that for the other atoms. The *z*-polarized OH motion is not much in evidence, but would appear to be at around 330 cm^{-1}, while the corresponding *x*,*y*-polarized motions are around 220 cm^{-1}. However, the degree of mixing and overlap is so high as to suggest that it is somewhat artificial to separate out individual components in the range below 400 cm^{-1}.

Note that Table 3b is derived without reference to the vi-

brational mode calculations. It is also important to note that vibrational mode calculations give the harmonic values required by the force field, whereas the molecular dynamics simulations give the frequency of actual motion in the force field for classical, thermally activated oscillators with amplitude range determined by temperature. An attempt to improve the simulation by running at lower temperature merely led to deterioration in the signal to noise ratio, no doubt associated with the smaller amplitudes of motion.

Comparison of molecular dynamics simulation and vibrational mode analysis

The agreement between these two approaches is good but not perfect. The use of a finite supercell imposes constraints on the results of the vibrational mode analysis as determined by simulations of different-sized supercells. The vibrational mode analysis relies on the energy-minimized structure and effectively represents brucite at absolute zero temperature. The harmonic approximation used in the analysis focuses on the potential energy at the bottom of the potential energy well. In contrast, the molecular dynamics results are comparatively noisy and appear to be modulated by the excursions in potential energy with the

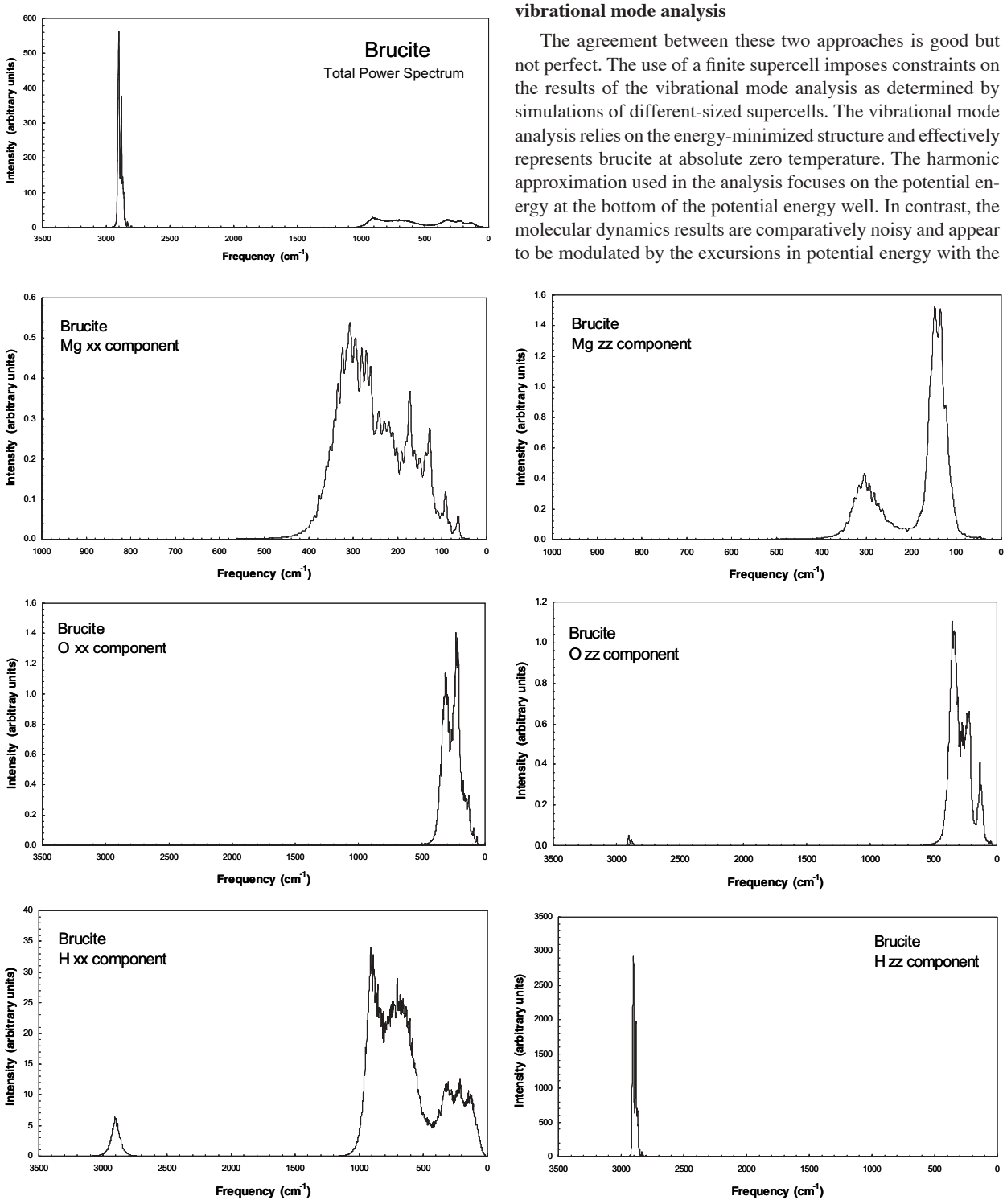

FIGURE 4. Power spectra (total, *xx*, and *zz* components) for Mg, O, and H in a simulated $8 \times 6 \times 3$ brucite supercell at 300 K.

addition of thermal energy to the brucite. Given these constraints, the agreement is satisfactory.

The modes from the vibrational mode analysis can be individually examined. However, only in the simplest cases does it seem possible to directly relate the results of molecular dynamics simulation to specific modes, and then only in a general sense. Thus we can presume that the bimodal distribution of *z*-polarized H atom motions in the high frequency region is directly related to the distribution of available modes, but (given the essentially random nature of classical thermal motions) there seems no way of breaking down the dynamics simulation results into motions where OH groups above and below the plane are moving in or out of phase.

However, one result, which we regard as the most important to emerge from this work (see below), is quite unambiguously shown by both approaches: the existence of an extensive, infrared silent, group of MOH bending motions in the region 500–1000 cm^{-1}.

Relationship to experimental data

Classically, each degree of freedom has mean energy $kT/2$, so that 300 K corresponds to an approximate energy of 115 cm^{-1}. Thus, except at the lowest frequencies, the energies assigned in the simulations will fall considerably short of those in the first vibrational excited state, so that the data from dynamics simulations should be compared with harmonic frequencies rather than the (somewhat lower) directly observable frequencies. The vibrational mode analysis, of course, also gives harmonic frequencies. These are not, however, generally available, and we make do with the observed frequencies instead. Many workers have measured these, and (despite difficulties such as the presence of impurities in mineral samples; see Frost and Kloprogge 1999) a consensus appears to have emerged (Lutz et al. 1994). Very recently, some of these assignments have been called into question (de Oliveira and Hase 2001) on the basis of isotopic shift data; in view of the current limitations of our force field, we do not attempt to adjudicate this dispute. In addition, several inelastic neutron scattering experiments have been performed on brucite, most recently by Chakoumakos et al. (1997). Spectral frequencies and assignments from these sources are collected in Table 5.

If we bear in mind that the CLAYFF model is a low level of theory, developed with no explicit inclusion of vibrational data, the agreement between Tables 2 and 3 on the one hand, and Table 5 on the other, is surprisingly good, with the difference between the calculated and observed values being of the order of 10–15% or less (20% in the case of the infrared-active T_z(OH) motion).

There is one notable exception, and that is the infrared-active MOH bending mode, calculated at 85 cm^{-1} but observed at 415 (or perhaps 462) cm^{-1}. We can immediately attribute this failure of our model to its major known conceptual shortcoming, namely the absence of any explicit MOH angular constraint. Although CLAYFF has an option to explicitly include MOH three-body interactions, we chose not to constrain the hydroxyl energetics and therefore rely on the implicit and aggregate effect of the nonbonded contributions on the angle bend behavior. Additionally, use of a nonbonded three-body term with the simulation software has led to significant slowdown in execution and to instabilities while accounting for appropriate three-body interactions.

TABLE 5. Summary of literature frequencies (cm^{-1})

Mode		Lutz et al. 1994	de Oliveira and Haase 2001	Chakoumakos et al. 1997
OH stretch:	A_{1g}	3654		
	A_{2u}	3698	3698	3770*
OH rotation:	E_g	725		
(MOH bend)	E_u	415	462†	383
OH T_{xy} (MOM	E_g	280		
bend/stretch)	E_u	361	368†	
OH T_z (MOM	A_{1g}	444		
stretch/bend)	A_{2u}	455	562	
E_u acoustic				125
Combination or unassigned				305, 780, 925, 1060

* Unresolved pair.
† Mixed modes.

In our molecular model, the partial charge on Mg is +1.05, and not the full formal charge of 2.0 electron charge units, implying a considerable degree of covalency in the Mg-O bond. Elementary theory then predicts something approaching sp^3 hybridization at O, and the existence of covalent (not merely electrostatic) forces directing the OH bond along the local threefold axis.

One highly significant feature of all our supercell dynamics runs and force field calculations is the prediction of the existence of a large number of spectroscopically silent MOH bending motions higher in frequency than the E_g vibration of this type. This is not, for us, an unexpected result. The separation between the E_u and E_g vibrations arises here from the repulsion between H atoms in adjacent layers on different sheets, but in both these motions, the OH groups within each layer move in phase and avoid each other. However, when we allow for the motions in which adjacent fundamental unit cells within the simulation supercells are not constrained to be in phase, we expect (and find) higher frequency motions in which OH groups within the same layer are forced toward each other.

We invoke these higher frequency motions to explain the observed strong neutron scattering reported by Chakoumakos et al. (1997) in the region 700–1100 cm^{-1}, which otherwise needs to be explained in terms of combination modes. In much the same spirit, the unassigned neutron scattering at 305 cm^{-1} can be attributed to the high density of spectroscopically silent vibrations of all kinds in this region.

CONCLUDING REMARKS

We conclude as follows:

(1) On the whole, both molecular dynamics, and vibrational mode analysis using an appropriately sized supercell as a repeating unit, give what appear to be acceptable qualitative accounts of the vibrational motions of brucite. The explicitly calculated vibrational mode frequencies are, however, distorted by unrealistic constraints on the phase difference between adjacent unit cells, while the power spectra derived from the dynamics simulation show major low-frequency modulations, which may be computational artifacts or may represent the superposition of very low frequency vibrations.

(2) Our results appear to favor the traditional assignments (Lutz et al. 1994), rather than those more recently suggested by de Oliveira and Hase (2001), although we do not regard this conclusion as definitive.

(3) We claim to have removed the mystery of the existence of strong neutron scattering in the region 700–1100 cm^{-1}. We suspect that this explanation also applies to the observed (Kagunya et al. 1998) neutron scattering behavior of hydrotalcite phases.

(4) There is absolutely no relationship in brucite between the positions of highest density of states within a band of frequencies, and the position of any spectroscopically active modes within that band. This is a consequence of the symmetry rules, the special nature ($k = 0$) of the spectroscopically active fundamentals, and the delocalization of the vibrational modes in general throughout the crystal.

(5) Thus, it appears that the results of this research may have been achieved at a certain cost. We and others have used density of vibrational states as a tool for analyzing the far infrared spectra of hydrotalcite. It may be that such a procedure is justified in that case, since the interlayer region of hydrotalcite is highly disordered and, as a result, the vibrational modes are somewhat localized, but this point requires further investigation. Regarding minerals with regular structures, especially where there are strong interactions between atoms in adjacent fundamental simulation cells, correspondence between spectroscopic observables and overall density of states cannot safely be taken for granted.

ACKNOWLEDGMENTS

We thank the U. S. Department of Energy, Office of Basic Energy Sciences, Geosciences Research for funding to RTC. Sandia is a multiprogram laboratory operated by Sandia Corporation, a Lockheed Martin Company, for the United States Department of Energy's National Nuclear Security Administration under contract DE-AC04-94AL85000. We acknowledge support from the Welch Foundation (grant no. B-1445), and Development Leave support from the University of North Texas. P.S.B. is an associate member of the Pennsylvania State University Astrobiology Research Center.

REFERENCES CITED

Born, M. and Huang, K. (1954) Dynamical Theory of Crystal Lattices. Oxford University Press, London.

Buchanan, R.A., Caspers, H.H., and Murphy, J. (1963) Lattice vibration spectra of $Mg(OH)_2$ and $Ca(OH)_2$. Applied Optics, 2, 1147–1150.

Chakoumakos, B.C., Loong, C.-K., and Schultz, A.J. (1997) Low-temperature structure and dynamics of Brucite. Journal of Physical Chemistry B, 101, 9458–9462.

Cotton, F.A. (1990) Chemical Applications of Group Theory, 3rd Edition. Wiley-Interscience, New York.

Cygan, R.T. (2001) Molecular modeling in mineralogy and geochemistry. In R.T. Cygan and J.D. Kubicki, Eds., Molecular Modeling Theory: Applications in the Geosciences, 42, p. 1–35. Reviews in Mineralogy and Geochemistry, Mineralogical Society of America, Chantilly, Virginia.

Cygan, R.T., Liang, J.-J., and Kalinichev, A.G. (2004) Molecular models of hydroxide, oxyhydroxide, and clay phases and the development of a general force field. Journal of Physical Chemistry B, 108, 1255–1266.

Dawson, P., Hadfield, C.D., and Wilkinson, G.R. (1973) Polarized infrared and Raman spectra of magnesium hydroxide and calcium hydroxide. Journal of Physics and Chemistry of Solids, 34(7), 1217–1225.

de Oliveira, E.F. and Hase, Y. (2001) Infrared study and isotopic effect of magnesium hydroxide. Vibrational Spectroscopy, 25(1), 53–56.

Desgranges, L., Calvarin, G., and Chevrier, G. (1996) Interlayer interactions in $M(OH)_2$: a neutron diffraction study of $Mg(OH)_2$. Acta Crystallographica, Section B: Structural Science, B52, 82–86.

Desiraju, G.R. (2002) Hydrogen bridge is in crystal engineering: interactions without borders. Accounts of Chemical Research, 35, 565–573.

Frost, R.L. and Kloprogge, J.T. (1999) Infrared emission spectroscopic study of brucite. Spectrochimica Acta, Part A: Molecular and Biomolecular Spectroscopy, 55A, 2195–2205.

Hoover, W.G. (1985) Canonical dynamics: Equilibrium phase-space distributions. Physical Review A, 31(3), 1695–1697.

Kagunya, W., Baddour-Hadjean, R., Kooli, F., and Jones, W. (1998) Vibrational modes in layered double hydroxides and their calcined derivatives. Chemical Physics, 236, 225–234.

Kruger, M.B., Williams, Q., and Jeanloz, R. (1989) Vibrational spectra of brucite $[Mg(OH)_2]$ and portlandite $[Ca(OH)_2]$ under pressure. Journal of Chemical Physics, 91, 5910–5915.

Kubicki, J.D. (2001) Interpretation of vibrational spectra using molecular orbital theory calculations. In R.T. Cygan and J.D. Kubicki, Eds., Molecular Modeling Theory: Applications in the Geosciences, 42, p. 459–484. Reviews in Mineralogy and Geochemistry, Mineralogical Society of America, Chantilly, Virginia.

Lutz, H.D., Moeller, H., and Schmidt, M. (1994) Lattice vibration spectra. Part LXXXII. Brucite-type hydroxides $M(OH)_2$ (M = Ca, Mn, Co, Fe, Cd)óIR and Raman spectra, neutron diffraction of $Fe(OH)_2$. Journal of Molecular Structure, 328, 121–132.

Mitra, S.S. (1962) Vibration spectra of solids. Solid State Physics, 13, 1–80.

Newman, S.P., Greenwell, H.C., Coveney, P.V., and Jones, W. (2001) Computer modelling of layered double hydroxides. In V. Rives, Ed., Layered Double Hydroxides, 93–114. Nova Science Publishers, Inc., Huntington, New York.

Parrinello, M. and Rahman, A. (1981) Polymorphic transitions in single crystals: A new molecular dynamics method. Journal of Applied Physics, 52(12), 7182–7190.

Pracht, G., Weckler, B., and Lutz, H.D. (2003) Diffuse reflection infrared fourier transform (DRIFT) spectra and high-temperature DRIFT spectra of β-$Ni(IO_3)_2H_4H_2O$, $Ni(IO_3)_2H_2H_2O$, $Mg(OH)_2$, and Zn(OH)F: Novel embedding materials. Applied Spectroscopy, 57, 1254–1259.

Ryskin, Y.I. (1974) The vibrations of protons in minerals: Hydoxyl, water and ammonium. In V.C. Farmer, Ed., The Infrared Spectra of Minerals, chapter 9, p. 137–181. Mineralogical Society, London.

Safford, G., Brajovic, V., and Boutin, H. (1963) An investigation of the energy levels in alkaline earth hydroxides by inelastic scattering of slow neutrons. Physics and Chemistry of Solids, 24, 771–777.

Tosi, M.P. (1964) Cohesion of ionic solids in the Born model. Solid State Physics, 131, 533–545.

Ugliengo, P., Pascale, F., Merawa, M., Labeguerie, P., Tosoni, S., and Dovesi, R. (2004) Infrared spectra of hydrogen-bonded ionic crystals: Ab initio study of $Mg(OH)_2$ and β-$Be(OH)_2$. Journal of Physical Chemistry B, 108, 13632–13637.

Verlet, L. (1967) Computer experiments on classical fluids: I. Thermodynamical properties of Lennard-Jones molecules. Physical Review, 159, 98–103.

Wang, J., Kalinichev, A.G., Amonette, J.E., and Kirkpatrick, R.J. (2003) Interlayer structure and dynamics of Cl-bearing hydrotalcite: Far infrared spectroscopy and molecular dynamics modeling. American Mineralogist, 88, 398–409.

Weckler, B. and Lutz, H.D. (1996) Lattice vibration spectra, Part LXXXIX. Near-infrared spectra of M(OH)Cl (M = Ca, Cd, Sr), Zn(OH)F, γ-$Cd(OH)_2$, $Sr(OH)_2$, and brucite-type hydroxides $M(OH)_2$ (M = Mg, Ca, Mn, Fe, Co, Ni, Cd). Spectrochimica Acta, Part A: Molecular and Biomolecular Spectroscopy, 52A, 1507–1513.

Zigan, F. and Rothbauer, R. (1967) Neutronenbeugungsmessungen am brucit. Neues Jahrbuch für Mineralogie, 137–143.

MANUSCRIPT RECEIVED SEPTEMBER 19, 2005
MANUSCRIPT ACCEPTED MARCH 5, 2006
MANUSCRIPT HANDLED BY KEVIN ROSSO